Journal of Molecular Liquids 334 (2021) 116390

Contents lists available at ScienceDirect

Journal of Molecular Liquids

journal homepage: www.elsevier.com/locate/molliq

Green synthesis of novel $CuCo_2O_4$ nanocomposite for stable hybrid supercapacitors by deep eutectic solvents

Surendra.K. Shinde [a], Swapnil S. Karade [b], Nagesh C. Maile [c], Hemraj.M. Yadav [a], Gajanan S. Ghodake [a], Ajay.D. Jagadale [d], Dae-Young Kim [a,*]

[a] Department of Biological and Environmental Science, College of Life Science and Biotechnology, Dongguk University, Biomedical Campus, 32 Dongguk-ro, Ilsandong-gu, Siksa-dong, Goyang-si, Gyeonggi-do, 10326, South Korea
[b] Electrochemical Energy Laboratory, Department of Chemical and Biomolecular Engineering, Yonsei University, Seoul, Republic of Korea
[c] Department of Environmental Engineering, Kyungpook National University, 80 Daehak-ro, Buk-gu, Daegu 41566, Republic of Korea
[d] Center for Energy Storage and Conversion, School of Electrical and Electronics Engineering, SASTRA Deemed University, Thanjavur 613401, Tamil Nadu, India

ARTICLE INFO

Article history:
Received 22 February 2021
Revised 25 April 2021
Accepted 1 May 2021
Available online 5 May 2021

Keywords:
$CuCo_2O_4$
Thin films
Deep eutectic solvents
Nanograin
Specific capacity
Hybrid supercapacitor

ABSTRACT

Currently, many transition metal oxides (TMOs) have been demonstrated as attractive nanomaterials for application in supercapacitors for energy storage/conversion systems. Among TMOs, $CuCo_2O_4$ has presented excellent electrochemical properties, including higher electrical behavior. Also, they are readily accessible in earth, ecofriendly and cost effective compared to other nanocompunds. In this research, we have for the first time synthesized $CuCo_2O_4$ (CCO) nanomaterials using a deep eutectic solvents (DES) method for supercapacitor (SC) applications. We systematically studied the effect of annealing temperature of CCO on its structural, morphological, and electrical properties. The CCO was annealed at different temperature of 150, 200, 250, and 300 °C for 3 h. CCO annealed at 250 °C exhibited the superior performance compared to other as-synthesized and annealed samples. The optimized CCO electrode shows outstanding supercapacitive properties with specific capacity 421 mAh g^{-1} at 10 mV s^{-1}, excellent GCD capability, and super cycling stability. This indicates that the DES-prepared CCO shows better electrochemical performance due to highly porous nanostructure providing more active sites for easy transformation of the ions.

1. Introduction

Supercapacitors (SCs) are the core component in the development of sustainable energy storage systems with high power density, high energy density, fast charge–discharge, long life, cycling stability, and low cost [1–4]. SCs can be classified into two categories based on the charge storage mechanism: electrical double layer capacitors (EDLCs), which consist of electrostatic charge accumulation at the electrode/electrolyte interfaces, and pseudocapacitors, which comprise reversible Faradic reactions. Pseudocapacitors deliver much higher specific capacitance and energy density than the EDLC [5–7] Metal oxides of copper, nickel, cobalt, and manganese have gained increasing attention in SCs research because of their electrochemical properties [8,9]. Copper oxide and cobalt oxide has many potential applications in various scientific technologies. Among numerous metal oxides, binary transition metal oxides (TMOs) of copper and cobalt showed excellent electrochemical properties, such as specific capacitance, conductivity, cycling performance, and structural stability [10].

The earth abundant spinel type cobalt oxide and its derived compounds offer a promising alternative cheap material for electrochemical energy storage application because of its high theoretical capacitance ~ 3600 F g^{-1}, electrochemical reversibility, and stability. However, the electrochemical performance was slightly lower than expected due to the internal low conductivity, morphology, surface area, chemical composition, and crystallinity [11,12]. Recently, many efforts have been devoted to overcoming these obstacles by designing mixed-metal oxides, controlling morphology, size, and structural properties. Previous reports found that the introduction of Cu in the host cobalt oxide could be beneficial towards improving conductivity and electrochemical properties. Therefore, copper cobalt-based oxides have been highlighted because of their natural abundance, excellent stability, and low cost. Furthermore, amalgamation of metal oxides is a promising way to boost electrical conductivity, electro-chemical properties, and structural stability.

* Corresponding author.
E-mail address: sbpkim@dongguk.edu (D.-Y. Kim).

https://doi.org/10.1016/j.molliq.2021.116390
0167-7322/

Recently, many CCO based electrodes with various morphologies, such as nanoparticles [13], nanoarrays [5], nanowires [14], nanorods [15], nanoneedles [16], and nanosheets [17], and cedar leaf-like [18], dandelion-like [19] nanoforests [20], and these nanostructures were considered to have a key influence on the electrochemical performance. Among the reported synthesis methods, CCO have been mostly synthesized by a hydrothermal method. However, in this work, we have synthesized CCO by using a deep eutectic solvents (DES) method for hybrid SCs application on Ni foam. The effect of annealing temperature on the structural, morphological, and electrochemical properties of the CCO electrodes showed that the CCO nanomaterials positively affected with annealing temperature. The structural, morphological, and supercapacitive performance revealed that CCO electrodes annealing temperature at 250 °C achieves the superior performance compared to other as-synthesized and annealed samples, which may be due to the better crystallinity, higher porosity, and lower grain size. This indicates that the sample annealed at 250 °C provided easy pathways like highways for ion transport or ion exchange during the electrochemical reaction. The sample annealed at 250 °C achieved a specific capacity 421 mAh g^{-1} at 10 mV s^{-1}, which is higher than that of the as-synthesized and other annealed samples. This optimized sample was found to be more suitable for hybrid SCs applications because of their better electrical properties and higher active surface area.

2. Experimental

2.1. Materials

Analytical-grade chemicals such as choline chloride, urea, copper nitrate hexahydrate ($Cu(NO_3)_2$).$6H_2O$, and cobalt nitrate tri hydrate ($Co(NO_3)_2$).$3H_2O$ were purchased from Sigma Aldrich and used directly without further purification.

2.2. Preparation of deep eutectic solvent (DES)

Choline chloride and urea were added to a flask at a molar ratio of 1:2, and the mixture was constantly stirred at 60 °C. After some time, the entire solid mixture changed to a transparent liquid. The reaction was maintained for 1 h to ensure a stable liquid mixture of choline chloride/urea-based DES. The DES was transferred to an air-tight container and used as a solvent for further reactions.

2.3. Synthesis of $CuCo_2O_4$

For synthesis of $CuCo_2O_4$, 5 g $Cu(NO_3)_2{\cdot}6H_2O$ and 10 g $Co(NO_3)_2{\cdot}3H_2O$ were dissolved in a solution bath containing 40 mL DES with vigorous stirring for 15 min. After that, 40 mL deionized water was added, and the bath temperature set to 70 °C for 12 h with constant stirring to complete the reaction process. Then, the reaction was cooled to room temperature and the product filtered using vacuum filtration. The product was washed several times with deionized water followed by ethanol. Finally, the collected product was kept for drying in an oven for 12 h at 60 °C. Moreover, the post annealing effect on DES mediated as-synthesized CCO was studied at different temperatures of 150, 200, 250, and 300 °C for 3 h in air. The as-synthesized and post powder was used for the preparation of thin films on Ni foam using the drop coating method and further investigations were performed. The as-synthesized CCO thin films were air dried naturally for overnight and were further annealed at 100 °C for 10 min to vaporize the PVDF binder. Henceforth, the synthesized samples are denoted as CCO-RT, CCO-150, CCO-200, CCO-250, and CCO-300 for as-synthesized and annealed at 150, 200, 250, and 300 °C, respectively.

2.4. Growth mechanism

The growth mechanism of the CCO can be predicted as follows. In the present work we have prepared a DES by using choline chloride as quaternary ammonium salt and urea as a hydrogen bond donor. There is no any water influence during the preparation of DES [21,22]. Ammonia releases urea when heating the DES, which further reacts with the $Cu(NO_3)_2$ and $Co(NO_3)_2$ and forms the Cu and Co ammonium nitrate.

$$CO(NH_2)_2 \rightarrow NH_3 + HCNO \quad [1]$$

$$Cu(NO_3)_2 + NH_3 \rightarrow Cu(NH_3)(NO_3)_2 \quad [2]$$

$$Co(NO_3)_2 + NH_3 \rightarrow Co(NH_3)(NO_3)_2 \quad [3]$$

Further, addition of water in the reaction bath initiates the reaction towards the formation of CCO. During the reaction, the aggregation of the CCO nanostructure in the form of clustered nanoparticles.

$$Cu(NH_3)(NO_3)_2 + 2Co(NH_3)(NO_3)_2 + 4H_2O \rightarrow CuCo_2O_4 + 3NH_4NO_3 + 3HNO_3 + H_2 \uparrow \quad [4]$$

2.5. Characterization

The structures of the as-synthesized and composite nanomaterials were confirmed using powder X-ray diffraction (XRD, Bruker D8 Advanced). X-ray photoelectron spectroscopy (XPS) was used to determine the chemical composition and elemental information (ULVAC-PHI Quantera SXM). The surface morphologies of the as-synthesized and composite samples were studied using field emission scanning electron microscopy (FE-SEM; JEOL JSM-7100) and high-resolution transmission electron microscopy (HR-TEM; JEOL JEM-2100). The SC properties were investigated using a three-electrode system with the as-synthesized electrodes, Pt, and Ag/AgCl as the working, counter, and reference electrode, respectively. Electrochemical analyses consisting of cyclic voltammetry (CV), galvanostatic charge–discharge (GCD), and electrochemical impedance spectroscopy (EIS) were carried out on a Versa STAT 3 machine in 3 M KOH. The electrochemical tests for CV and GCD were performed at scan rates and current densities of 10–100 mV s^{-1} and 10–50 mA cm^{-2}, respectively. The EIS studies were performed within the frequency range of 0.1–100 kHz.

The specific capacity (Cs) of the CCO electrodes was calculated with the formulas below for the CV curves [23,24];

$$C_s(C\ g^{-1}) = \frac{\int I(V)dV}{m\nu} \quad [5]$$

$$C_s(mAh\ g^{-1}) = \frac{\int I(V)dV}{m\nu \times 3.6} \quad [6]$$

where, '$\int$I(V)dv' is the area under the CV curve, 'm' is the active electrode mass loading on the substrate, and 'ν' is the scan rate. Similarly, the specific capacity of the electrode can be calculated using charge–discharge profile as given in the below eqs. (7) and (8).

$$C_s(C\ g^{-1}) = \frac{I\int Vdt}{mV} \quad [7]$$

$$C_s(mAh\ g^{-1}) = \frac{I\int Vdt}{mV \times 3.6} \quad [8]$$

where, "I" is the discharge current density, '$\int Vdt$' is the area covered by the discharge curve, '*m*' is the active mass loading on the substrate, and '*V*' is the potential window.

3. Results and discussion

SEM analysis was used for the study of the surface properties of the as-synthesized and annealed CCO composites nanomaterials. Fig. 1 present the SEM images of the as-synthesized and annealed CCO nanocomposite materials with different magnifications. All SEM images of as-synthesized and annealed CCO presented uniform formation of the nanograin-like nanoparticles and drastic change in its porosity, grain size, and compactness of after annealing CCO [25,26]. Fig. 1 (a, b) shows the SEM images of the as-synthesized CCO composites with different magnifications. The SEM images of as-synthesized CCO show the e-regular growth developed on the surface of nanomaterials and the annealed samples shown in Fig. 1 (c-j) [27,28]. After annealing as-synthesized CCO samples at 150 °C, surface of nanomaterials shows the drastic change from irregular growth to compact growth, and aggregation of nanograins uniformly covers the surface, as shown in Fig. 1 (c, d). Furthermore, we changed annealing temperature from 150 to 200 °C, the surface morphology shows quite similar nanostructures, but with reduced particle size from 45-35 to 35–25 nm, respectively (as shown in the Fig. 1f). However, for CCO-250 sample, surface of the nanomaterials shows highly porous nanograins/nanosheet-like hybrid nanostructures developed with lower size of nanograins compared to the other CCO samples [29-32]. The grain size of the optimized CCO-250 sample is 15–10 nm, which indicates that these sample provided more surface area than the other samples due to its lower size and highly porous structure. The high porosity and lower particle size of the nanomaterials are more benefits, because these types of surface provided easy paths, so called super highways, for the ions and electrons transferred during electrochemical study. After higher temperature annealing at 300 °C, surface of samples shows the highly compact and cubic-like nanostructures, as shown in Fig. 1 (i, j). Thus, we confirmed that optimized CCO-250 sample annealing at 250 °C is the best annealing temperature for the optimization of the nanomaterial for the electrochemical application. The SEM analyses are very helpful by the optimization and support the structural, and supercapactive properties of the CCO nanomaterials [33].

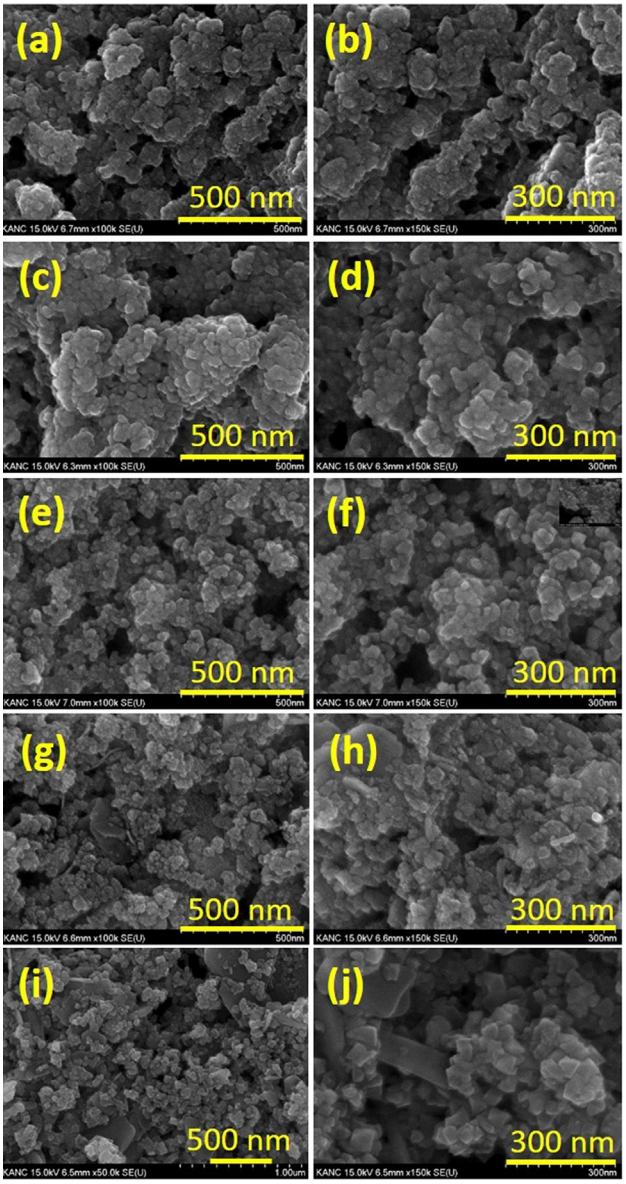

Fig. 1. FE-SEM of as- synthesized CCO-RT, CCO-150, CCO-200, CCO-250, and CCO-300 samples with different magnifications.

For further analysis, CCO-RT and CCO-250 nanocomposites were investigated by TEM. Fig. 2 (a-c) and Fig. 3 (ac) present a typical TEM analysis of the CCO-RT and CCO-250 nanocomposites with various magnifications, respectively. CCO-RT has nanoparticles-like nanostructures; interconnected and developed chain-like nanoparticles with sizes 7–10 nm (Fig. 2b). The pin hole like dark/white nanoparticles with highly porous surface was observed at high magnification as shown in Fig. 2 (c). This indicates that the CCO-RT is porous, and porous nanoparticle-like nanostructures are useful to provide active surface area to capably interface between the electrode/electrolyte and for faster transformation of ion/electron. This is very useful for the improved the electrochemical activities as well as the rate-stable material, which is a very important factor in the supercapcitor application [34]. The elemental distribution and composition of the CCO-RT was further studied by the elemental mapping and EDS, respectively. The mapping results show the identical distribution of Cu, Co, and O elements are presented on the surface of the CCO-RT in the Fig. 2(e-h). EDS results confirmed the existence Cu, Co, and O elements with stoichiometry ratio, it indicates the pure phase formation of the CCO-RT nanomaterials (as shown in the Fig. 2i). Fig. 3 (a-d) shows the TEM images of the CCO-250 at a various magnifications. Fig. 3 (e-h) presented a highly porous nanoparticles are uniformly covered on the surface of interconnected nanosheet-like nanostructures [35]. This type of hybrid arrangement of the nanostructures provided effective involvement of surface area and could be useful for the improving the SC performance and electrical stability of the ternary metal oxides (CCO).

The width and length of CCO-250 was in the range of 40–50 and 80–100 nm for the nanosheet, respectively and the diameters of the nanoparticles was about 10 nm. To study the more detailed information of the crystallographic nature of CCO sample, we examined the selected area electron diffraction (SAED) the patterns of both samples, which was shown in the inset of the Fig. 2i and Fig. 3i. The SAED patterns showed the black dark rings of the diffraction and white dots, which indicates the polycrystalline nature of the CCO-RT and CCO-250 sample [36]. The HR-TEM images of the CCO-RT and CCO-250 are shown in the Fig. 2d and 3d, the lattice fringes between two fringes are 0.28 and 0.23 nm, with a cubic crystal phase, respectively [34,35].

Surface area of the active material is an important parameter to accounting a supercapacitor performance which was determined by using Brunauer-Emmet-Teller (BET) analysis. Fig. 4 shows the

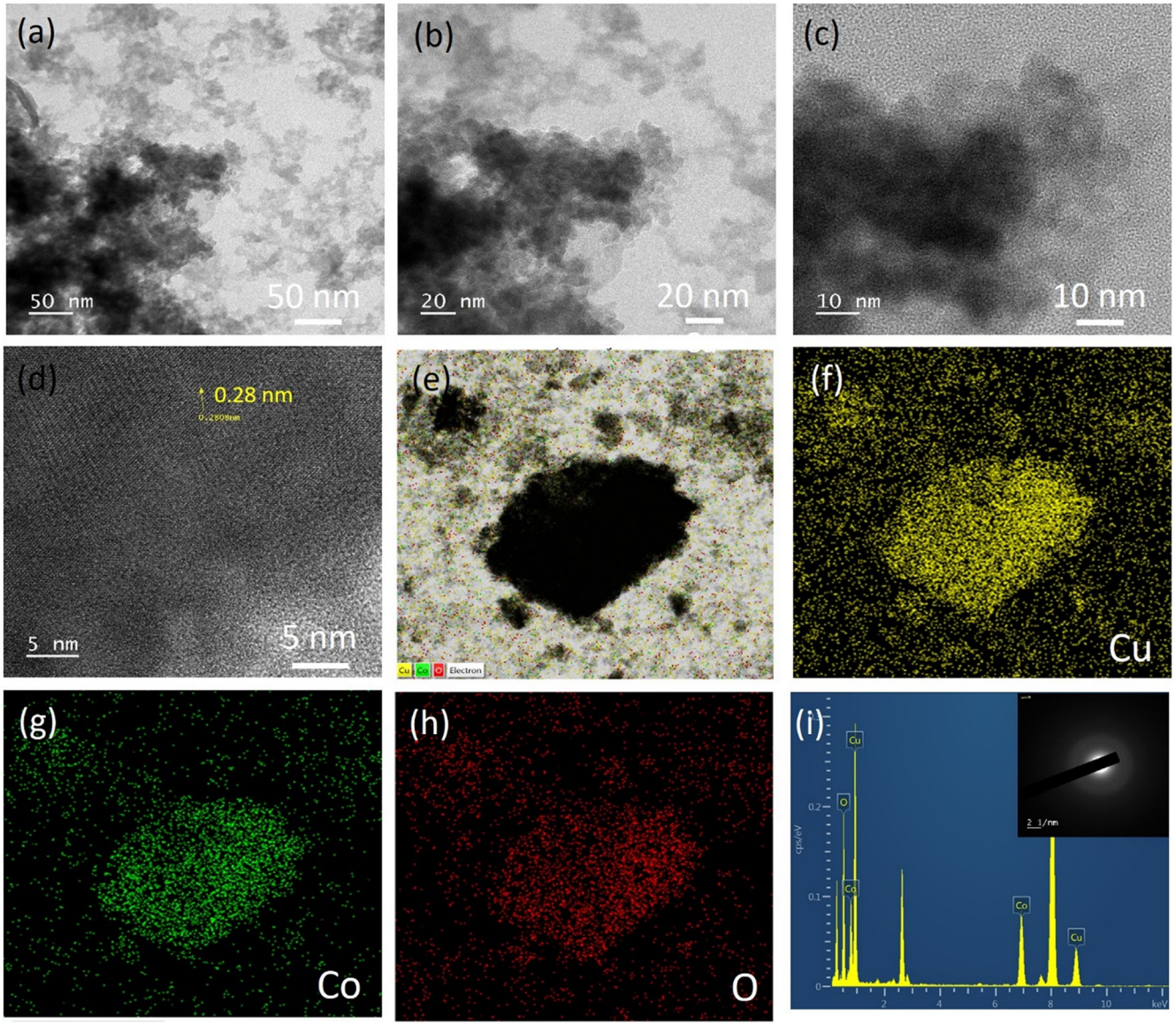

Fig. 2. (a-c) TEM images, (d) HR-TEM images, (e-h) elemental mapping, and (i) EDS of as-synthesized CCO-RT sample, inset shows the SEAD patterns.

N_2 adsorption/desorption isotherm of the CCO-RT and CCO-250. It reveals classical type-VI adsorption/desorption isotherm, strongly suggests mesoporous surface area of both samples. The surface area of the CCO-RT and CCO-250 was found to be 9 and 16 m^2 g^{-1}, respectively. Thus, the CCO-250 shows the higher surface area as compared to the CCO-RT sample. This type's hybrid nanostructure with higher active surface area is more beneficial for supercapacitors application as it provide easy path to electron transformation as well as small pores diameters [37] which sturdily assisted for high electrochemical performance of the $CuCo_2O_4$ electrode.

The phase purities and identification of crystal structure of the all as-synthesized and all annealed CCO samples were investigated using the XRD. Fig. 5a reveals the XRD patterns of the CCO-RT, CCO-150, CCO-200, CCO-250, and CCO-300, respectively. XRD patterns clearly shows the improvement in the crystallinity with annealing treatment. CCO-150 shows almost similar crystal structural and phase with CCO-RT. Furthermore, as we increased annealing temperature from 150 to 200 °C, CCO-200 samples shows the improvement in the peak intensity and crystallinity [38]. Thus, these results indicate the the structural properties of the CCO was altered with annealing temperature. However, after increasing annealing temperature up to 250 °C, the XRD patterns shows the better and higher crystallinity, it suggest that 250 °C is sufficient to higher crystallinity and better development of the formation of pure phase [38,39]. The diffraction patterns of the CCO reveal that higher sharpness and better crystallinity annealed at 250 °C, which confirms the polycrystalline nature with pure phase of cubic crystal structure of the CCO-250 [40]. The further increment in the annealing temperature up to 300 °C, shows the hybrid phase of cubic $CuCo_2O_4$ and orthorhombic phase of $CoCu_2O_3$. Figure 5a presents the diffraction peaks at 32.31, 36.64, 38.70, 47.50, 56.35, and 65.60, 69.60° assigned to (2 2 0), (3 1 1), (2 2 2), (4 0 0), (4 2 2), (4 4 0) and (5 3 1) planes are well matched to standard JCPDS cards of cubic phase of $CuCo_2O_4$ (JCPDS No. 001–1155), which was shown in the XRD diffraction patterns of CCO-RT to CCO-200. The diffraction peaks at 28.64, 30.21, 35.57, 41.62, 49.55, 53.81, 62.64, and 65.8° related to the (0 0 1), (1 0 1), (0 1 1), (2 1 1), (2 2 0), (4 1 1), (0 1 2) and (2 1 2) planes of the orthorhombic phase of $CoCu_2O_3$ (JCPDS No. 76–04442). The diffraction patterns of higher annealing temperature show the mixed phase of $CuCo_2O_4$ and $CoCu_2O_3$ nanomaterials which was shown

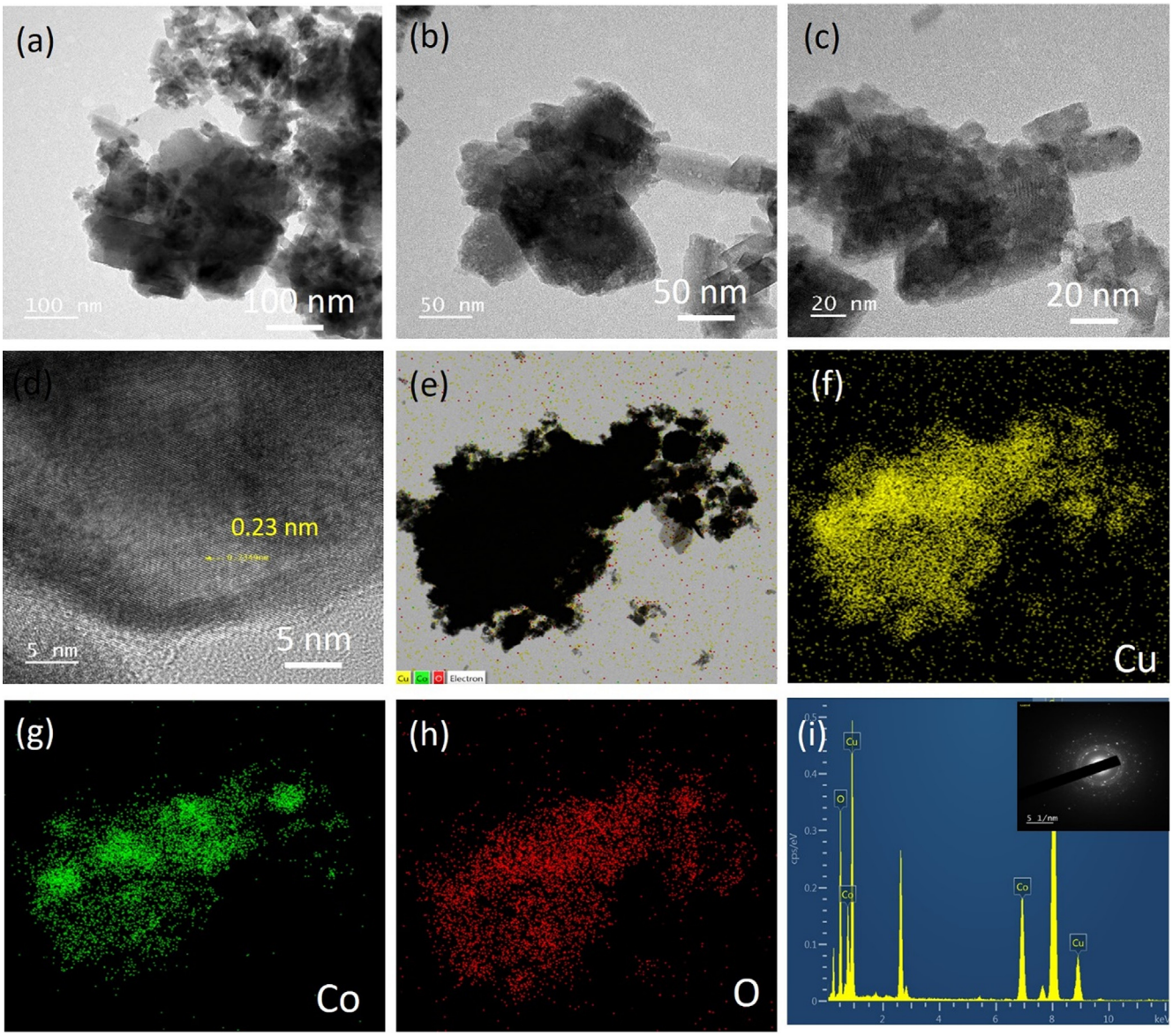

Fig. 3. (a-d) TEM images, (d) HR-TEM images, (e-h) elemental mapping, and (i) EDS of optimized CCO-250 sample, inset shows the SEAD patterns.

in the Fig. 5a . There was no any binary phase of copper oxide and cobalt oxide formed, indicating the formation of phase pure as well as hybrid $CuCo_2O_4$ and $CoCu_2O_3$ heterostructures [34]. No other phase observed, it indicates that the CCO samples are highly pure and unique. Similar results have been reported previously for other materials with different applications [41,42].

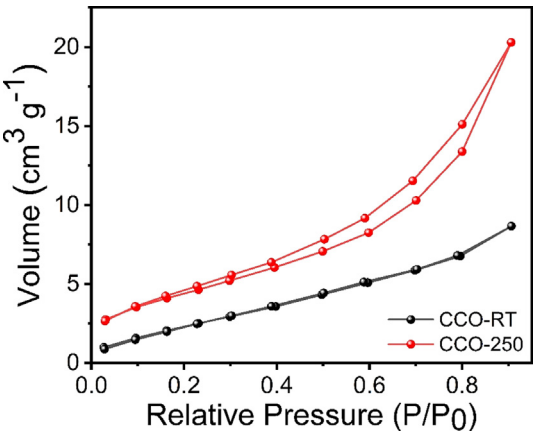

Fig. 4. BET plots of as-synthesized and optimized CCO sample at 250 °C, respectively.

Fig. 5b presented the XPS survey scan spectra of the CCO-RT and CCO-250, respectively. The survey spectra presented the existence of Cu, Co, and O elements, which indicates the formation of the $CuCo_2O_4$ material in both samples. Fig. 5 (c-e) presents the core levels spectra of the Cu 2p, Co 2p, and O1s, respectively. The core level spectrum of Cu 2p, shows two main characteristics peaks located at 932.55 and 952.53 eV, corresponding to the Cu $2p_{3/2}$ and Cu $2p_{1/2}$, respectively [43]. The splitting difference between the binding energies of the Cu $2p_{3/2}$ and Cu $2p_{1/2}$ is about 19.9 eV. Moreover, we noticed that two more characteristics peaks, which are related to the shake-up satellites peaks of the Cu $2p_{3/2}$ and Cu $2p_{1/2}$, respectively. The satellites peaks located at 941.7 and 962.35 eV, which indicates the presence of Cu^{2+} [44]. Similarly, core level spectra of the Co 2p shows the two main characteristics peaks at 780.94 and 796.76 eV, which correspond to the Co $2p_{3/2}$ and Co $2p_{1/2}$, respectively. The difference between the two main peaks is around 15.82 eV, which suggest the Co^{2+} and Co^{3+}

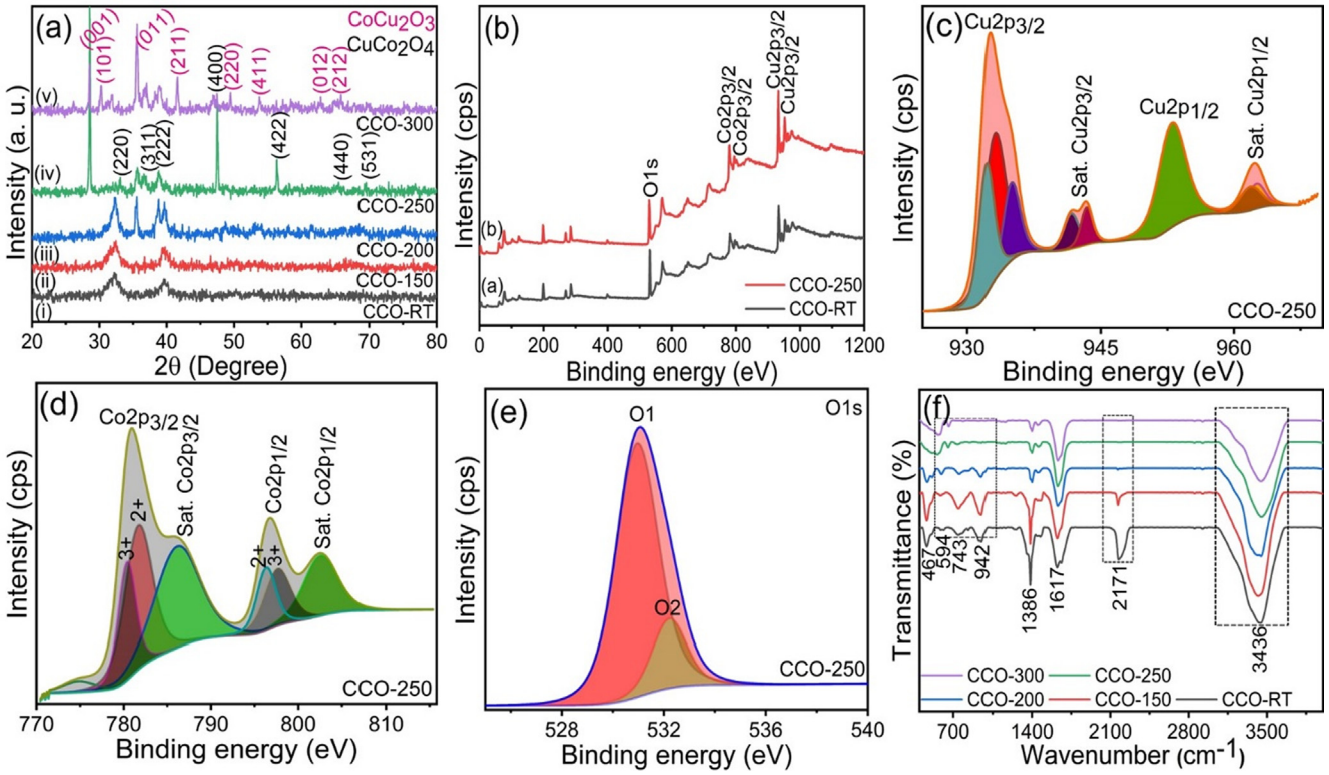

Fig. 5. (a) XRD patterns of CCO-RT, CCO-150, CCO-200, CCO-250, and CCO-300 samples, (b) XPS survey spectra of as-synthesized and optimized CCO-250 sample, (c) core level of Cu 2p, (d) core level of Co 2p, (e) core level of O 1 s, (f) FT-IR spectra of the CCO-RT, CCO-150, CCO-200, CCO-250, and CCO-300 samples.

oxidation states [45,46]. Additionally, Fig. 5e presents the O 1 s spectrum, which demonstrates two peaks at 531.06 and 532.29 eV, which are related to the metal–oxygen bonds, which indicates the presence of oxygen ions [45,47]. These XPS results clearly show the development of ternary CCO.

The existence of functional moieties on the surface of as-synthesized and annealed CCO was confirmed by FT-IR analysis. Fig. 5f presents the FT-IR spectra of as-synthesized and annealed CCO composites. The strong absorption peaks observed at 3436 cm^{-1}, which are correlated to the OH-containing of water molecule, present in the OH modes, are presented in the as-synthesized and lower annealing temperature [48]. Furthermore, at higher annealing temperature, we clearly observed that the peak intensity of the 3436 cm^{-1} is reduced; in addition, some absorption bonds are vanished at higher temperature shown in the FT-IR by mark. This indicates the different annealing temperatures have positively affected on the ternary composite of the CCO. The broad absorption peaks noticed at the 467 cm^{-1} and 500–594 cm^{-1}, which correspond to the stretching vibrational modes of Co–O and Cu–O, respectively [49,50]. These two vibrational bonds indicate the mixed metal oxides materials are present in all CCO samples. From the of FT-IR results of CCO composites, the existence of two main vibration modes at 467 and 594 cm^{-1}, confirmed the formation of pure phase with annealing temperature of CCO and this is in strong support to the XRD results.

4. Electrochemical study

After confirming the effect of the annealing temperature on the structural, morphology, and composition of CCO, we studied the effect of annealing temperature on the electrochemical properties of the as-synthesized CCO electrodes. Fig. 6 (a-e) presents the CV curves of the CCO-RT, CCO-150, CCO-200, CCO-250, and CCO-350 electrodes with a various scan rates from 10 to 100 mV s^{-1}, in the potential window 0 to 0.5 V, respectively. The current values of about 25, 57, 60, 300, and 140 mA cm^{-2} were observed for CCO-RT, CCO-150, CCO-200, CCO-250, and CCO-350 electrodes, respectively. Annealed CCO's shown more current values compared with CCO-RT, demonstrating that the temperatures are positively affecting on the electrochemical performance [47]. From all CV curve, the current density of annealing CCO electrodes increased progressively with the increasing annealing temperature and higher annealing temperature the values of current density decreased, due to the compact nanostructure. The CCO-250 had the higher current density indicating that this sample provides the higher capacitance values than the other CCO samples which may be due to the structural deformation and this electrochemical analysis was in good agreement with the SEM results [39]. The CCO-RT electrode was incapable to provide all sites involved in the electrochemical reaction, furthermore the samples prepared at low annealing temperature shows the poor crystallinity which ultimately affected on the electrical conductivity. The optimum annealing temperature of 250 °C for CCO offering more active sites, high surface area, and highly porous structure than the other samples. Also, the better crystallinity of CCO-250 with phase purity gives better electrical conductive and higher electrochemical performance [51]. The CCO-250 exhibits very intense change in the current distribution with well distinguished redox peaks and depicts enhanced electrochemical performance. The possible charge–discharge reaction is as follows.

$$CuCo_2O_4 + OH^- + H_2O \rightleftharpoons CuOOH + 2CoOOH + e^- \quad [9]$$

In point of fact, the current in the CV curve is the combination of surface charge (Q_s) contribution due to electrostatic charge adsorption as well as faradaic reaction on the surface of the electrode and diffusion controlled (Q_d) processes allied with surface and bulk electrochemical reaction. The charge storage mechanism can be easily understood using power law.

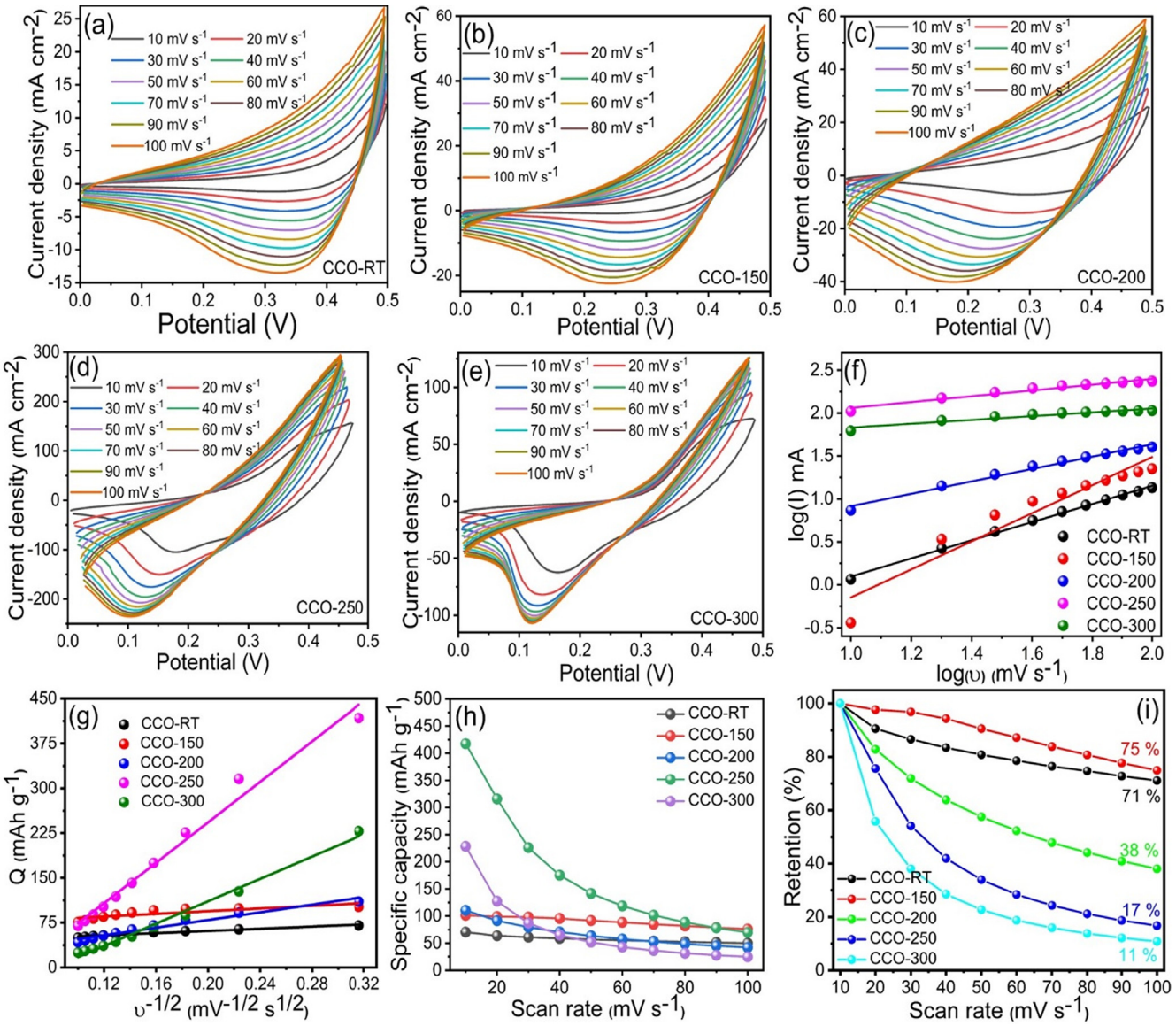

Fig. 6. (a-e) CV curves of CCO-RT, CCO-150, CCO-200, CCO-250, and CCO-300 electrodes at various scan rates, respectively, (f) log of peak current as a function of the log of scan rate, (g) total charge Q_t as a function of reciprocal square root of scan rate, contribution from Q_s and Q_d to the Q_t stored at different scan rates, (h) specific capacity of CCO-RT, CCO-150, CCO-200, CCO-250, and CCO-300 electrodes with different scan rates, (i) capacity retention of the CCO-RT, CCO-150, CCO-200, CCO-250, and CCO-300 electrodes with different scan rates.

$$I = a v^b \quad [10]$$

Where, I is current associated with electrode in CV, ν is the scan rate, a and b are the adjustable parameters having definite conditions. When b is equal to 1 then charge storage kinetics purely capacitive in nature with surface adsorption of electrolyte ions, when b value is below 0.5 then the electrode possesses purely battery type nature with diffusion-controlled process in dominance whereas if the b value is in between 0.5 and 1 then the nature of charge storage includes both surface and diffusion-controlled processes. The value of b can be calculated using the plot of log(i) vs log(ν) as showing in Fig. 6f. The as-synthesized and annealed electrodes (at 150, 200, 250 and 300 °C) shows b values of 1.06, 1.63, 0.72, 0.34, and 0.22, respectively. Based on Trasatti plot [52] in the frame of total charge (Q_t) and inverse square root of the scan rate, we can easily find the dominant charge storage mechanism during the charge storage (Fig. 6g). The as-synthesized and low-temperature annealed (150 °C) electrodes exhibit capacitive dominant in the charge storage, with further increased annealing temperature shifting the charge storage mechanism towards diffusion-controlled processes. Utilizing all possible sites of the electrode with bulk faradaic redox processes the CCO electrode annealed at 250 °C showed very high specific capacity (Cs) of 421 mAh g^{-1} at lower scan rate of 10 mV s^{-1} with respect to the other electrodes (Fig. 6h). Fig. 6h shows the obtained values of the Cs with respect to the various scan rates for all samples. The calculated values of the Cs were 70, 101, 110, 421, and 228 mAh g^{-1} for the CCO-RT, CCO-150, CCO-200, CCO-250, and CCO-300 electrodes, respectively. The obtained values of Cs indicate the CCO-250 electrode show the higher values than the other electrode, indicating the nanograins provided more active sites, high surface area, high porosity, and provided easy path to ion transformation from one layer to other [39]. Fig. 6i shows retention in the Cs value as a function if scan rate ranging from 10 to 100 mV s^{-1} for all CCO electrodes. It reveals the capacitive dominant electrodes showed superior rate capability by retaining 75% of the capacity even at

higher scan rate 100 mV s^{-1} while the diffusion-controlled dominant electrodes (250 °C and 300 °C) showed very poor rate capability of 17% and 11%. These results are in good agreement with the XRD and SEM analyses. This implies the redox activity of the CCO material was improved and particle dimensions was reduced with increased annealing temperature from 150 to 250 °C. However, further increase in the annealing temperature up to 300 °C resulted into the poor electrochemical performance due to the binary and unstable phase of CCO-300.

Fig. 7 (a-e) present the GCD measurements of the as-synthesized and annealed CCO electrodes in the potential ranging from 0.0 to 0.5 V with different current densities range 10–50 mA cm^{-2}. The GCD curves shows the charging/discharging time of CCO-RT, CCO-150, CCO-200, CCO-250, and CCO-300 are 118, 28, 109, 600, and 136 s, respectively. These results indicate the CCO-250 electrode shows the higher electrochemical capacitance, which may be due to the better crystallinity, high surface area, and high porosity with more electroactive sites [47,53]. The GCD curves demonstrate the as-synthesized and annealed CCO electrode possesses the pseudocapacitive nature and the good reversibility, which may be due to the reversible faradaic redox reaction [54]. The Cs values of the CCO-RT, CCO-150, CCO-200, CCO-250, and CCO-300 are calculated to be 119, 135, 225, 394, and 156 mAh g^{-1} at current density 10 mA cm^{-2}, respectively (Fig. 7f). The calculated values of Cs of the CCO-250 shows the higher electrochemical performance than the as-synthesized and other annealed CCO electrodes. Fig. 7g and Fig. 7h shows the coulombic efficiency and cycling stability of CCO electrode, respectively. Fig. 7h shows the cycling stability of the synthesized and optimized CCO electrodes, respectively. The retention capacity indicates optimized CCO electrodes annealed at 250 °C shows the better than the synthesized CCO electrode, which suggest that annealing temperatures are positively affected on the ternary compound $CuCo_2O_4$ [55]. Table 1 depicts the higher performance of CCO-250 electrode compared with previous results. The preparation of ternary CCO by DLS method would be a superior option for developing electrodes in energy storage systems.

The EIS analysis were used to investigate the relation between the electrical conductivity and interface between the electrodes/-electrolyte of the as-synthesized and annealed CCO samples with

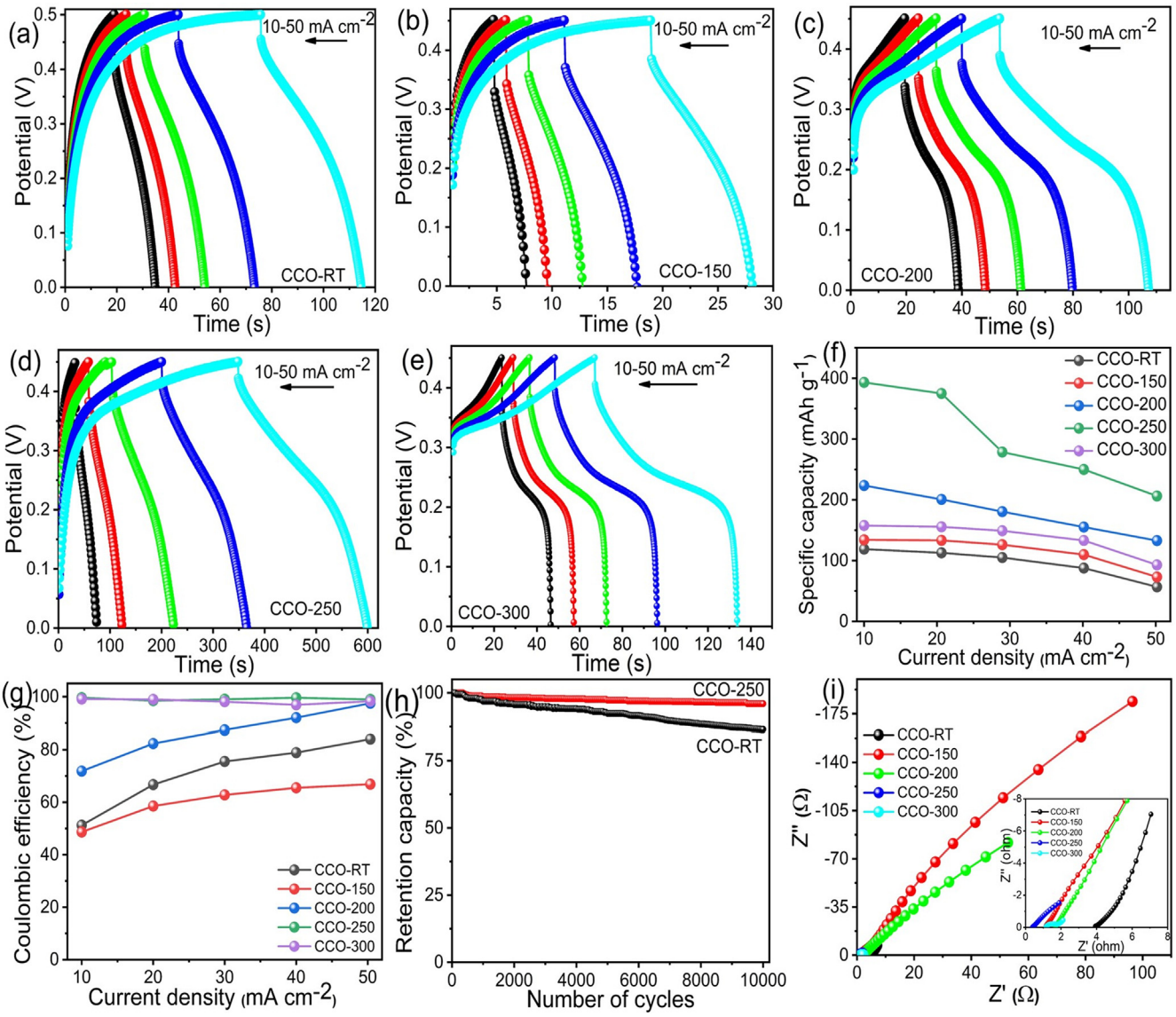

Fig. 7. (a-e) GCD curves of CCO-RT, CCO-150, CCO-200, CCO-250, and CCO-300 electrodes at different current densities, respectively, and (f) specific capacity with respect to the current density, (g) coulombic efficiency of CCO-RT, CCO-150, CCO-200, CCO-250, and CCO-300 electrodes with different current densities, respectively. (g) Cycling stability of the of CCO-RT, and CCO-250 electrodes, (i) Nyquist plots of CCO-RT, CCO-150, CCO-200, CCO-250, and CCO-300 electrodes.

Table 1
The electrochemical performance of $CuCo_2O_4$ as supercapacitor electrodes.

Materials	Electrode (Foam)	Method	Potential window (V)	Specificcapacity (mAh g^{-1})	Current density	Electrolyte(M KOH)	Capacity retention (%)	Cycles	Reference
$CuCo_2O_4$	Ni	DES	0–0.5	421	10 mA cm^{-2}	3	92	10,000	This study
$CuCo_2O_4$	Ni	Hydrothermal	0–0.4	136.42	5 mA cm^{-2}	3	95.4	1000	[5]
$CuCo_2O_4$	Ni	Electrodeposition	0–0.4	163.66	1 A g^{-1}	3	93	5000	[17]
$CuCo_2O_4$	Ni	Hydrothermal/	−0.1–0.4	169.88	1.08 A g^{-1}	2	88	2000	[18]
$CuCo_2O_4$	Ni	annealing	0–0.47	346.84	1 mA cm^{-2}	6	92.32	5000	[19]
$CuCo_2O_4$	Ni		0–0.4	91.11	2 mA cm^{-2}	2	94	1500	[20]
$CuCo_2O_4$	Ni	Hydrothermal	0–0.4	177.22	1 A g^{-1}	6	85.1	4600	[56]
$CuCo_2O_4$@CQDs	Ni		0–0.55	233.56	1 A g^{-1}	2	91	4000	[59]
$CuCo_2O_4$	Ni		0–0.5	139.72	1 A g^{-1}	3	85.5	10,000	[60]

a frequency ranges from 0.1 to 10 MHz at a potential amplitude of 3.9 mV. Fig. 7i shows the Nyquist plots of the as-synthesized and CCO electrodes annealed at 150, 200, 250 and 300 °C. Inset shows the zoom area of the Nyquist plots and it clearly indicates the CCO-250 shows the lower solution and charge transfer resistance than the all other electrodes. The obtained values of R_S for the as-synthesized and CCO electrode annealed at 150, 200, 250, and 300 °C are 3.87, 1.11, 1.65, 0.36, and 1.12 Ω, respectively. The calculated values of the charge transfer resistance (R_{ct}) of the CCO-RT and CCO electrode annealed at 150, 200, 250, and 300 °C are 5.29, 10.42, 25.04, 0.11, and 0.66 Ω, respectively. Out of obtained values of R_s and R_{ct} indicates the CCO-250 shows the lower values of the charger transfer resistance and solution resistance resulted into superior electrochemical SC performance [57, 58]. The lower values of the R_s and R_{ct} for CCO-250 may be attributed to the typical nanostructure, phase purity, higher active surface area, highly porous nature, and excellent redox properties of the porous ternary CCO electrode [47,55].

5. Conclusion

In conclusion, we designed a novel $CuCo_2O_4$ (CCO) nanomaterial synthesized by deep eutectic solvents method for the SC application. In this work, we demonstrated the improvement in the structural, morphological, and electrochemical properties of $CuCO_2O_4$ using different annealing temperatures. The annealing effect on electrochemical properties is discussed along with particle size, phase purity, porosity, and surface area. Annealing at 300 °C promotes formation of binary phase and poor supercapacitor performance while annealing at 250 °C demonstrated pure phase formation and superior supercapacitor performance of $CuCO_2O_4$. The $CuCO_2O_4$ electrode obtained at 250 °C shows higher specific capacity, 421 mAh g^{-1}, at constant current density than the other four electrodes. Finally, the electrochemical properties of $CuCO_2O_4$ can be tunned with different annealing temperature.

Declaration of Competing Interest

The authors declare that they have no known competing financial interests or personal relationships that could have appeared to influence the work reported in this paper.

Acknowledgments

Analysis of samples was supported by Dongguk University, Seoul, Korea Research Fund 2020–2022. ADJ is thankful to the Department of Science and Technology (DST), Govt. of India for financial assistance under the DST INSPIRE Faculty Scheme [DST/INSPIRE/04/2017/002737].

References:

[1] A. Aljaafari, N. Parveen, F. Ahmad, M.W. Alam, S.A. Ansari, Self-assembled Cube-like Copper Oxide Derived from a Metal-Organic Framework as a High-Performance Electrochemical Supercapacitive Electrode Material, Sci. Rep. 9 (2019) 1–10, https://doi.org/10.1038/s41598-019-45557-6.
[2] S.A. Ansari, N. Parveen, H.M. Kotb, A. Alshoaibi, Hydrothermally derived three-dimensional porous hollow double-walled Mn2O3 nanocubes as superior electrode materials for supercapacitor applications, Electrochim. Acta. 355 (2020), https://doi.org/10.1016/j.electacta.2020.136783 136783.
[3] S.A. Ansari, N.A. Khan, Z. Hasan, A.A. Shaikh, F.K. Ferdousi, H.R. Barai, N.S. Lopa, M.M. Rahman, Electrochemical synthesis of titanium nitride nanoparticles onto titanium foil for electrochemical supercapacitors with ultrafast charge/discharge, Sustain. Energy Fuels. 4 (2020) 2480–2490, https://doi.org/10.1039/d0se00049c.
[4] P.H. Wadekar, R.V. Khose, D.A. Pethsangave, S. Some, The Effect of Bio-inspired Co-electrolytes for Enhancement of Electrochemical Properties of Supercapacitors, ENERGY Environ. Mater. 3 (2020) 429–435, https://doi.org/10.1002/eem2.12097.
[5] Q. Gao, J. Wang, J. Wang, Morphology-controllable synthesis of CuCo2O4 arrays on Ni foam as advanced electrodes for supercapacitors, J. Alloys Compd. 789 (2019) 193–200, https://doi.org/10.1016/j.jallcom.2019.03.041.
[6] S.A. Ansari, M.H. Cho, Growth of three-dimensional flower-like SnS2 on g-C3N4 sheets as an efficient visible-light photocatalyst, photoelectrode, and electrochemical supercapacitance material, Sustain. Energy Fuels. 1 (2017) 510–519, https://doi.org/10.1039/c6se00049e.
[7] M.P. Bondarde, P.H. Wadekar, S. Some, Synthesis of sulfur doped carbon nanoparticle for the improvement of supercapacitive performance, J. Energy Storage. 32 (2020), https://doi.org/10.1016/j.est.2020.101783 101783.
[8] P.H. Wadekar, R.V. Khose, D.A. Pethsangave, S. Some, Waste-Derived Heteroatom-Doped Activated Carbon/Manganese Dioxide Trio-Composite for Supercapacitor Applications, Energy Technol. 8 (2020) 1901402, https://doi.org/10.1002/ente.201901402.
[9] P.H. Wadekar, R.V. Khose, D.A. Pethsangave, S. Some, One-step Preparation of Conducting Polymer/Metal Oxide Doped RGO Trinary Composite for Supercapacitor Applications, ChemistrySelect. 5 (2020) 11769–11777, https://doi.org/10.1002/slct.202002911.
[10] E. Karaca, K. Pekmez, N.Ö. Pekmez, Electrosynthesis of polypyrrole-vanadium oxide composites on graphite electrode in acetonitrile in the presence of carboxymethyl cellulose for electrochemical supercapacitors, Electrochim. Acta. 273 (2018) 379–391, https://doi.org/10.1016/J.ELECTACTA.2018.04.059.
[11] P. Sivakumar, M. Jana, M. Kota, M.G. Jung, A. Gedanken, H.S. Park, Controllable synthesis of nanohorn-like architectured cobalt oxide for hybrid supercapacitor application, J. Power Sources. 402 (2018) 147–156, https://doi.org/10.1016/J.JPOWSOUR.2018.09.026.
[12] J. Yang, H. Liu, W.N. Martens, R.L. Frost, Synthesis and Characterization of Cobalt Hydroxide, Cobalt Oxyhydroxide, and Cobalt Oxide Nanodiscs, J. Phys. Chem. C. 114 (2010) 111–119, https://doi.org/10.1021/jp908548f.
[13] R. BoopathiRaja, M. Parthibavarman, A. Nishara Begum, Hydrothermal induced novel CuCo2O4 electrode for high performance supercapacitor applications, Vacuum. 165 (2019) 96–104, https://doi.org/10.1016/j.vacuum.2019.04.013.
[14] A. Pendashteh, S.E. Moosavifard, M.S. Rahmanifar, Y. Wang, M.F. El-Kady, R.B. Kaner, M.F. Mousavi, Highly Ordered Mesoporous CuCo2O4 Nanowires, a Promising Solution for High-Performance Supercapacitors, Chem. Mater. 27 (2015) 3919–3926, https://doi.org/10.1021/acs.chemmater.5b00706.
[15] Q. Li, R. Hu, J. Qi, Y. Sui, Y. He, Q. Meng, F. Wei, Y. Ren, Y. Zhao, Facile synthesis of mesoporous CuCo2O4 nanorods@MnO2 with core-shell structure grown on RGO for high-performance supercapacitor, Mater. Lett. 249 (2019) 151–154, https://doi.org/10.1016/j.matlet.2019.04.043.
[16] L. Zhang, R. Li, R. Li, W. Li, R. Li, C. Li, Y. Zhou, CuCo2O4nanoneedle array with high stability for high performance asymmetric supercapacitors, RSC Adv. 10 (2020) 22775–22782, https://doi.org/10.1039/d0ra03771k.
[17] S.M. Pawar, B.S. Pawar, P.T. Babar, A.T.A. Ahmed, H.S. Chavan, Y. Jo, S. Cho, J. Kim, B. Hou, A.I. Inamdar, S.N. Cha, J.H. Kim, T.G. Kim, H. Kim, H. Im, Nanoporous CuCo 2 O 4 nanosheets as a highly efficient bifunctional electrode for supercapacitors and water oxidation catalysis, Appl. Surf. Sci. 470 (2019) 360–367, https://doi.org/10.1016/j.apsusc.2018.11.151.

[18] Y. Wang, D. Yang, J. Lian, J. Pan, T. Wei, Y. Sun, Cedar leaf-like CuCo2O4 directly grow on nickel foam by a hydrothermal/annealing process as an electrode for a high-performance symmetric supercapacitor, J. Alloys Compd. 735 (2018) 2046–2052, https://doi.org/10.1016/j.jallcom.2017.12.005.
[19] M. Lan, B. Liu, R. Zhao, M. Dong, X. Wang, L. Fang, L. Wang, Dandelion-like CuCo2O4 arrays on Ni foam as advanced positive electrode material for high-performance hybrid supercapacitors, J. Colloid Interface Sci. 566 (2020) 79–89, https://doi.org/10.1016/j.jcis.2020.01.077.
[20] Y. Wang, D. Yang, J. Lian, T. Wei, Y. Sun, Ordered corn-like CuCo2O4 nanoforests covering Ni foam for a high-performance all-solid-state supercapacitor, J. Alloys Compd. 741 (2018) 527–531, https://doi.org/10.1016/j.jallcom.2018.01.168.
[21] S.S. Karade, S. Lalwani, J.H. Eum, H. Kim, Deep eutectic solvent-assisted synthesis of RuCo2O4: An efficient positive electrode for hybrid supercapacitors, Sustain. Energy Fuels. 4 (2020) 3066–3076, https://doi.org/10.1039/d0se00340a.
[22] P.H. Wadekar, R.V. Khose, D.A. Pethsangave, S. Some, One-Pot Synthesis of Sulfur and Nitrogen Co-Functionalized Graphene Material using Deep Eutectic Solvents for Supercapacitors, ChemSusChem. 12 (2019) 3326–3335, https://doi.org/10.1002/cssc.201900953.
[23] A.M. Patil, X. An, S. Li, X. Yue, X. Du, A. Yoshida, X. Hao, A. Abudula, G. Guan, Fabrication of three-dimensionally heterostructured rGO/WO3·0.5H2O@Cu2S electrodes for high-energy solid-state pouch-type asymmetric supercapacitor, Chem. Eng. J. 403 (2021), https://doi.org/10.1016/j.cej.2020.126411 126411.
[24] S.K. Shinde, H.M. Yadav, G.S. Ghodake, A.D. Jagadale, M.B. Jalak, D.-Y. Kim, Novel and efficient hybrid supercapacitor of chemically synthesized quaternary 3D nanoflower-like NiCuCo2S4 electrode, Ceram. Int. (2021), https://doi.org/10.1016/j.ceramint.2021.02.134.
[25] S.K. Shinde, G.S. Ghodake, N.C. Maile, H.M. Yadav, A.D. Jagadale, M.B. Jalak, A.A. Kadam, S. Ramesh, C. Bathula, D.-Y. Kim, Designing of nanoflakes anchored nanotubes-like MnCo2S4/halloysite composites for advanced battery like supercapacitor application, Electrochim. Acta. 341 (2020), https://doi.org/10.1016/j.electacta.2020.135973 135973.
[26] S.K. Shinde, M.B. Jalak, G.S. Ghodake, N.C. Maile, V.S. Kumbhar, D.S. Lee, V.J. Fulari, D.-Y. Kim, Chemically synthesized nanoflakes-like NiCo2S4 electrodes for high-performance supercapacitor application, Appl. Surf. Sci. 466 (2019) 822–829, https://doi.org/10.1016/J.APSUSC.2018.10.100.
[27] S.K. Shinde, D.P. Dubal, G.S. Ghodake, V.J. Fulari, Hierarchical 3D-flower-like CuO nanostructure on copper foil for supercapacitors, RSC Adv. 5 (2015) 4443–4447, https://doi.org/10.1039/C4RA11164H.
[28] S.K. Shinde, D.P. Dubal, G.S. Ghodake, D.Y. Kim, V.J. Fulari, Nanoflower-like CuO/Cu(OH)2 hybrid thin films: Synthesis and electrochemical supercapacitive properties, J. Electroanal. Chem. 732 (2014) 80–85, https://doi.org/10.1016/J.JELECHEM.2014.09.004.
[29] S. Shinde, H. Dhaygude, D.-Y. Kim, G. Ghodake, P. Bhagwat, P. Dandge, V. Fulari, Improved synthesis of copper oxide nanosheets and its application in development of supercapacitor and antimicrobial agents, J. Ind. Eng. Chem. 36 (2016) 116–120. doi:10.1016/J.JIEC.2016.01.038.
[30] S.K. Shinde, D.Y. Kim, G.S. Ghodake, N.C. Maile, A.A. Kadam, D.S. Lee, M.C. Rath, V.J. Fulari, Morphological enhancement to CuO nanostructures by electron beam irradiation for biocompatibility and electrochemical performance, Ultrason. Sonochem. 40 (2018) 314–322, https://doi.org/10.1016/j.ultsonch.2017.07.014.
[31] H.M. Yadav, G.S. Ghodake, D.-Y. Kim, S. Ramesh, N.C. Maile, D.S. Lee, S.K. Shinde, Nanorods to hexagonal nanosheets of CuO-doped manganese oxide nanostructures for higher electrochemical supercapacitor performance, Colloids Surfaces B Biointerfaces. 184 (2019), https://doi.org/10.1016/j.colsurfb.2019.110500 110500.
[32] S.K. Shinde, H.M. Yadav, S. Ramesh, C. Bathula, N. Maile, G.S. Ghodake, H. Dhaygude, D.-Y. Kim, High-performance symmetric supercapacitor; nanoflower-like NiCo2O4//NiCo2O4 thin films synthesized by simple and highly stable chemical method, J. Mol. Liq. 299 (2020), https://doi.org/10.1016/j.molliq.2019.112119 112119.
[33] S.K. Shinde, V.J. Fulari, D.-Y. Kim, N.C. Maile, R.R. Koli, H.D. Dhaygude, G.S. Ghodake, Chemical synthesis of flower-like hybrid Cu(OH)2/CuO electrode: Application of polyvinyl alcohol and triton X-100 to enhance supercapacitor performance, Colloids Surfaces B Biointerfaces. 156 (2017) 165–174, https://doi.org/10.1016/J.COLSURFB.2017.05.018.
[34] J. Sun, X. Du, R. Wu, Y. Zhang, C. Xu, H. Chen, Bundlelike CuCo2O4Microstructures Assembled with Ultrathin Nanosheets As Battery-Type Electrode Materials for High-Performance Hybrid Supercapacitors, ACS Appl. Energy Mater. 3 (2020) 8026–8037, https://doi.org/10.1021/acsaem.0c01458.
[35] W. Liu, H. Chen, H. Liao, K. Xiang, W. Chen, X. Li, Self-Supported Sisal-like CuCo2O4@Ni(OH)2 Core-Shell Composites Grown on Ni Foam for High-Performance All-Solid State Supercapacitors, Ind. Eng. Chem. Res. 58 (2019) 21233–21241, https://doi.org/10.1021/acs.iecr.9b04380.
[36] A.J.C. Mary, C.I. Sathish, A. Vinu, A.C. Bose, Electrochemical Performance of rGO/NiCo2O4@ZnCo2O4Ternary Composite Material and the Fabrication of an all-Solid-State Supercapacitor Device, Energy and Fuels. 34 (2020) 10131–10141, https://doi.org/10.1021/acs.energyfuels.0c01427.
[37] S.K. Shinde, D.P. Dubal, G.S. Ghodake, D.Y. Kim, V.J. Fulari, Morphological tuning of CuO nanostructures by simple preparative parameters in SILAR method and their consequent effect on supercapacitors, Nano-Structures & Nano-Objects. 6 (2016) 5–13, https://doi.org/10.1016/J.NANOSO.2016.01.004.
[38] A. Sadeghzadeh-Attar, M.R. Bafandeh, The effect of annealing temperature on the structure and optical properties of well-aligned 1D SnO2 nanowires synthesized using template-assisted deposition, CrystEngComm. 20 (2018) 460–469, https://doi.org/10.1039/c7ce01815k.
[39] G. Li, B. Song, X. Cui, H. Ouyang, K. Wang, Y. Sun, Y. Wang, Multidimensional and Binary Micro CuCo2O4/Nano NiMoO4 for High-Performance Supercapacitors, ACS Sustain. Chem. Eng. 8 (2020) 1687–1694, https://doi.org/10.1021/acssuschemeng.9b07356.
[40] A.R. Patel, G. Patel, G. Maity, S.P. Patel, S. Bhattacharya, A. Putta, S. Banerjee, Direct Oxidative Azo Coupling of Anilines Using a Self-Assembled Flower-like CuCo2O4Material as a Catalyst under Aerobic Conditions, ACS Omega. 5 (2020) 30416–30424, https://doi.org/10.1021/acsomega.0c03562.
[41] X. Li, M. Zhang, L. Wu, Q. Fu, H. Gao, Annealing temperature dependent ZnCo2O4 nanosheet arrays supported on Ni foam for high-performance asymmetric supercapacitor, J. Alloys Compd. 773 (2019) 367–375, https://doi.org/10.1016/j.jallcom.2018.09.197.
[42] J. Ungula, B.F. Dejene, H.C. Swart, Effect of annealing on the structural, morphological and optical properties of Ga-doped ZnO nanoparticles by reflux precipitation method, Results Phys. 7 (2017) 2022–2027, https://doi.org/10.1016/j.rinp.2017.06.019.
[43] H.M. Yadav, S.V. Otari, V.B. Koli, S.S. Mali, C.K. Hong, S.H. Pawar, S.D. Delekar, Preparation and characterization of copper-doped anatase TiO2 nanoparticles with visible light photocatalytic antibacterial activity, J. Photochem. Photobiol. A Chem. 280 (2014), https://doi.org/10.1016/j.jphotochem.2014.02.006.
[44] X. Xu, Y. Liu, P. Dong, P.M. Ajayan, J. Shen, M. Ye, Mesostructured CuCo2S4/CuCo2O4 nanoflowers as advanced electrodes for asymmetric supercapacitors, J. Power Sources. 400 (2018) 96–103, https://doi.org/10.1016/j.jpowsour.2018.08.012.
[45] J. Liang, M. Renzhi, N. Iyi, Y. Ebina, K. Takada, T. Sasaki, Topochemical synthesis, anion exchange, and exfoliation of Co-Ni layered double hydroxides: A route to positively charged Co-Ni hydroxide nanosheets with tunable composition, Chem. Mater. 22 (2010) 371–378, https://doi.org/10.1021/cm902787u.
[46] R. Ma, J. Liang, K. Takada, T. Sasaki, Topochemical synthesis of Co-Fe layered double hydroxides at varied Fe/Co ratios: Unique intercalation of triiodide and its profound effect, J. Am. Chem. Soc. 133 (2011) 613–620, https://doi.org/10.1021/ja1087216.
[47] V. Veeramani, R. Madhu, S.M. Chen, M. Sivakumar, Flower-Like Nickel-Cobalt Oxide Decorated Dopamine-Derived Carbon Nanocomposite for High Performance Supercapacitor Applications, ACS Sustain. Chem. Eng. 4 (2016) 5013–5020, https://doi.org/10.1021/acssuschemeng.6b01391.
[48] R. Abazari, A.R. Mahjoub, L.A. Saghatforoush, S. Sanati, Characterization and optical properties of spherical WO3 nanoparticles synthesized via the reverse microemulsion process and their photocatalytic behavior, Mater. Lett. 133 (2014) 208–211, https://doi.org/10.1016/j.matlet.2014.07.032.
[49] S.G. Hosseini, R. Abazari, A facile one-step route for production of CuO, NiO, and CuO-NiO nanoparticles and comparison of their catalytic activity for ammonium perchlorate decomposition, RSC Adv. 5 (2015) 96777–96784, https://doi.org/10.1039/c5ra20155a.
[50] L. Chen, L. Li, G. Li, Synthesis of CuO nanorods and their catalytic activity in the thermal decomposition of ammonium perchlorate, J. Alloys Compd. 464 (2008) 532–536, https://doi.org/10.1016/j.jallcom.2007.10.058.
[51] Y.-Q. Shao, Z.-Y. Yi, C. He, J.-Q. Zhu, D. Tang, Effects of Annealing Temperature on the Structure and Capacitive Performance of Nanoscale Ti/IrO_2-ZrO_2 Electrodes, J. Am. Ceram. Soc. 98 (2015) 1485–1492, https://doi.org/10.1111/jace.13475.
[52] S. Ardizzone, G. Fregonara, S. Trasatti, "Inner" and "outer" active surface of RuO2 electrodes, Electrochim. Acta. 35 (1990) 263–267, https://doi.org/10.1016/0013-4686(90)85068-X.
[53] N. Parveen, S.A. Ansari, S.G. Ansari, H. Fouad, N.M. Abd El-Salam, M.H. Cho, Solid-state symmetrical supercapacitor based on hierarchical flower-like nickel sulfide with shape-controlled morphological evolution, Electrochim. Acta. 268 (2018) 82–93. doi:10.1016/j.electacta.2018.01.100.
[54] F. Chen, Y. Ji, F. Ren, S. Tan, Z. Wang, Three-dimensional hierarchical core-shell CuCo2O4@Co(OH)2 nanoflakes as high-performance electrode materials for flexible supercapacitors, J. Colloid Interface Sci. 586 (2021) 797–806, https://doi.org/10.1016/j.jcis.2020.11.004.
[55] Y. Gai, T. Xie, Y. Shang, L. Su, J. Wang, L. Gong, Self-sacrificing template-derived hollow-structured NiCo2S4spheres with highly efficient supercapacitance performance, Energy and Fuels. 34 (2020) 10203–10210, https://doi.org/10.1021/acs.energyfuels.0c01957.
[56] Z. Wang, W. Qian, Y. Ran, P. Hong, X. Xiao, Y. Wang, Nanosheets based mixed structure CuCo2O4 hydrothermally grown on Ni foam applied as binder-free supercapacitor electrodes, J. Energy Storage. 32 (2020), https://doi.org/10.1016/j.est.2020.101865 101865.
[57] K. Xu, S. Ma, Y. Shen, Q. Ren, J. Yang, X. Chen, J. Hu, CuCo2O4 nanowire arrays wrapped in metal oxide nanosheets as hierarchical multicomponent electrodes for supercapacitors, Chem. Eng. J. 369 (2019) 363–369, https://doi.org/10.1016/j.cej.2019.03.079.
[58] J. Xie, Z. Zhan, S. Zhang, G. Li, H. Xia, Y. Yang, J. Xiong, CoMoO4 nanoplates decorated CuCo2O4 nanowires as advanced electrodes for high-performance

hybrid supercapacitors, Mater. Lett. 226 (2018) 30–33, https://doi.org/10.1016/j.matlet.2018.05.017.
[59] G. Wei, J. He, W. Zhang, X. Zhao, S. Qiu, C. An, Rational Design of Co(II) Dominant and Oxygen Vacancy Defective CuCo2O4@CQDs Hollow Spheres for Enhanced Overall Water Splitting and Supercapacitor Performance, Inorg. Chem. 57 (2018) 7380–7389, https://doi.org/10.1021/acs.inorgchem.8b01020.
[60] Y. Feng, W. Liu, Y. Wang, W. Gao, J. Li, K. Liu, X. Wang, J. Jiang, Oxygen vacancies enhance supercapacitive performance of CuCo2O4 in high-energy-density asymmetric supercapacitors, J. Power Sources. 458 (2020), https://doi.org/10.1016/j.jpowsour.2020.228005 228005.